arXiv:cond-mat/0104447v1 [cond-mat.str-el] 24 Apr 2001

Magnetothemopower study of quasi two-dimensional organic conductor α-(BEDT-TTF)$_2$KHg(SCN)$_4$

E. S. Choi
Department of Physics, Ewha Womans University, Seoul 120-750, Korea and National High Magnetic Field Laboratory, Florida State University, Tallahassee, Florida 32310

J. S. Brooks and J. S. Qualls*
National High Magnetic Field Laboratory and Physics Department, Florida State University, Tallahassee, Florida 32310

(Dated: February 1, 2008)

We have used a low-frequency magneto-thermopower (MTEP) method to probe the high magnetic field ground state behavior of α-(BEDT-TTF)$_2$KHg(SCN)$_4$ along all three principal crystallographic axes at low temperatures. The thermopower tensor coefficients (S_{xx}, S_{yx} and S_{zz}) have been measured to 30 T, beyond the anomalous low temperature, field-induced transition at 22.5 T. We find a significant anisotropy in the MTEP signal, and also observe large quantum oscillations associated with the de Haas - van Alphen effect. The anisotropy indicates that the ground state properties are clearly driven by mechanisms that occur along specific directions for the in-plane electronic structure. Both transverse and longitudinal magnetothermopower show asymptotic behavior in field, which can be explained in terms of magnetic breakdown of compensated closed orbits.

I. INTRODUCTION

The ground state of the quasi-two dimensional organic conductor α-(BEDT-TTF)$_2$KHg(SCN)$_4$ has emerged as one of the more important fundamental problems in the area of synthetic metals. This is due to the highly unusual magnetic field dependent behavior of the low temperature ground state which appears below a transition temperature $T_p = 8$ K. The band calculation and the Fermi surface study[1] suggest a two dimensional Fermi surface consisting of a quasi-one dimensional electron section and a closed hole pocket as shown in Fig. 1 (a). The density wave formation is believed to originate from the instability of the open orbit at low temperatures, which is followed by Fermi surface reconstruction[2]. This in turn leads to the unusual behavior of this compound at low temperatures and high magnetic field[3,4]. This ground state is now thought to be related to a charge density wave state where both spin and orbital mechanisms compete, as evidenced by recent studies in tilted magnetic fields[5,6]. Above 22.5 T an anomaly (called the "kink field" or B_k after its discovery by Osada et al.,[7] which appears in various transport-related measurements) occurs, and a new high field electronic state emerges. Recently the observation of critical state-like behavior in the magnetization[8] and susceptibility[9] above B_k has been reported, which indicates an unusual, highly conductive state which is associated with the Landau level filling fraction. Additional thermodynamic evidence for unusual, hysteretic behavior above B_k, which is related to the Landau level filling, has also been reported in high field magnetocaloric measurements[10].

The purpose of the present work has been to probe this novel ground state by thermoelectric power (TEP), which involves measuring the potential difference across a sample in the presence of a thermal gradient, as shown in Fig. 1 (c). In general, the resulting signal (in V/K) has the form[11]

$$S = \frac{\pi^2 k_B^2}{3e} T \left(\frac{d\ln n(E)}{dE} + \frac{d\ln v^2(E)}{dE} + \frac{d\ln \tau(E)}{dE}\right)|_{E=E_F} \quad (1)$$

where $n(E)$ is the density of the states, $v(E)$ is an average charge velocity, and $\tau(E)$ is the carrier scattering relaxation time. In addition, we have also measured the Nernst effect for specific sample configurations. This involves the transverse thermopower which is given in the simple approximation by $S_{xy} = QB(l/d)$, where Q is the Nernst coefficient, B is the magnetic field, and l/d is the ratio of the distance between the Nernst leads and the sample thickness. We note that ideally, for closed orbits, S_{xy} is not sensitive to electron/hole compensation effects, and that it increases linearly with magnetic field. (See discussion below).

Clearly the TEP and Nernst signals can be a complex mixture of phenomena which can be difficult to interpret, unless specific aspects of the system under consideration dominate and/or change dramatically[12]. Examples include the case of a conventional metal ($S \approx k_B/e\ k_BT/E_F$), a superconductor ($S = 0$), and the quantum Hall effect ($S \approx 0$ or a finite value depending on the Landau level filling). As we will show in the present case, the TEP probe for α-(BEDT-TTF)$_2$KHg(SCN)$_4$ is particularly sensitive to the Landau level spectrum, to the gap in the electronic structure, and to the in-plane electronic anisotropy.

In light of the discussion above, we state here the main findings of the present work before the full presentation. First, where comparisons can be made with previous studies (all of which are in-plane, and almost exclusively at low or zero magnetic fields), we find that our results agree in the details of the sensitivity of the thermopower

to the anisotropic Fermi surface topology, and with absolute value of the thermopower signals previously reported. In addition, we extend these measurements below T_p, where the TEP reveals details of the transition into the density wave state. Second, we observe, in the oscillatory METP, quantum oscillations associated with the main closed Fermi surface orbit frequency, and also oscillations associated with Fermi surface reconstruction and anomalous second harmonic signals which result from the density wave ground state. We believe that this is the first detailed study of quantum oscillations in a quasi-two dimensional organic conductor by thermopower methods. Third, the background (non-oscillatory) METP is sensitive to changes in the density wave ground state with magnetic field. This includes the signatures for three changes in the Fermi surface topology, one near 3.75 T, a second above 10 T, and a third above 22.5 T. The first two are associated with magnetic breakdown effects, and the latter is the first order phase transition to the high field state. The temperature-magnetic field phase diagram, based on the METP results, is presented. Fourth, we study in detail for the first time the inter-plane thermopower, which gives additional information about the role of the inter-plane transport mechanism of this material. Finally, in the high field state, we describe the phase relationship between the Nernst signal and the METP signal, which is consistent with theoretical predictions.

II. BACKGROUND

To our knowledge, no thermopower measurements have been carried out on the α-(BEDT-TTF)$_2$KHg(SCN)$_4$ material in very high magnetic fields. In 1950's, a series of calculations were done for high field dependence of magnetotransport properties. It was found that, in the limit of $\omega_c\tau \gg 1$ (where ω_c is the cyclotron frequency and τ is the scattering time), asymptotic magnetotranport properties (electrical conductivity[13], thermal conductivity[14] and thermopower[15]) are highly dependent on the Fermi surface topology and carrier compensation, while they weakly depend on the scattering time and the energy dispersion relations. It was therefore suggested that those measurements would be useful to reveal the Fermi surface topologies.

Due to the complex nature of thermopower signals in anisotropic materials, it is useful to briefly consider previous studies in organic materials, including those at high magnetic fields where field induced phase transitions occur. For consistency in the anisotropic thermopower parameters reported below, we use the following notation: the measured values can be written as S^{α}_{ij}, where $i, j = x$, y or z, signify that the heat current is applied along a geometrical direction j and the thermal emf is measured along a direction i, and α is one of the crystallographic axes along which the heat current is applied. For zero magnetic field, S^{α}_{ij} can be written in the reduced form such as S^{α}_{xx}, or simply S^{α}.

Mori et al.[16] performed the first in-plane measurements on α-(BEDT-TTF)$_2$KHg(SCN)$_4$, where the temperature dependence of S^a and S^c were found to be consistent with the topology of the hole and the electron bands (see Fig. 1). Here, in general, the TEP is positive when the thermal gradient is parallel to the open orbit sheets (where the closed hole orbits dominate the signal), and negative when the thermal gradient is perpendicular to the open orbit sheets (where the electron orbits are the main contribution). Our results, shown in Fig. 2 (and to be discussed below), are in reasonable agreement with these measurements. This assignment is supported by a simulation of the thermopower, based on Boltzmann transport theory, with the bandwidth parameters as input[16,17].

Another experiment involving in-plane thermopower has been performed on the 10.4 K organic superconductor[18] κ - (BEDT-TTF)$_2$Cu[N(CN)$_2$]Br (see also Gartner et al.[19] and Buravov et al.[20]). This system also has open and closed orbit Fermi surface bands, and again, the sign of the TEP in the normal state above T_c follows the general rule that it is positive when the thermal gradient is parallel to the electron sheets, and negative when perpendicular. Below T_c, the TEP vanished, as expected for a superconductor in zero magnetic field.

In studies of quasi-one dimensional (Q1D) systems based on the TCNQ charge transfer salts[21,22] and the perylene based compounds[23], various features of TEP were exhibited. Depending on the species of cations and the temperature range, they show linear temperature dependence, $1/T$ behavior, or temperature independence. The linear decrease of TEP was treated by a simple, single carrier in 1D tight binding band model, where the temperature behavior followed a linear T dependence, $S = 2\pi^2 k_B^2 T/3eW \cos(\pi/2\rho)/\sin^2(\pi/2\rho)$. Here W is the bandwidth and ρ is the number of carriers per site. Below the metal-to-insulator transition, the low temperature behavior followed the $1/T$ form $S = -(k_B/e)[(c-1)/(c+1)\, E_g/2k_BT + 3/4 \ln(m_e/m_h)]$ where E_g is the gap and c is the ratio of the electron to hole mobilities. The temperature independent thermopower with magnitude of $\sim \pm 60\mu$V/K was attributed to the spin configuration entropy ($\pm k_B/e$ (ln2)) in the strong Coulomb potential limit ($U \gg t$) in a quarter filled band.

In the presence of an applied magnetic field, the transverse thermopower (the Nernst effect) may be measured in addition to the normal longitudinal TEP (the Seebeck effect). Logvenov et al.[24] have investigated the superconducting states of two κ - (BEDT-TTF)$_2$X materials up to 3 T. The results, which showed non-zero TEP values even without magnetic fields, were interpreted in terms of flux motion and the Magnus force (in the case of the Nernst effect). The authors found considerable anisotropy which was attributed to the difference in the electron and hole Fermi surface sections.

The quasi-one dimensional Bechgaard salts, which ex-

hibit spin density wave (SDW) formation have been investigated by TEP and MTEP in some detail. The SDW transition in $(TMTSF)_2AsF_6$ at ambient pressure (T_{SDW}= 12 K) has been investigated[25] up to 11.3 T. Hysteretic temperature effects in the thermopower were observed as a function of field direction below T_{SDW}, and the authors speculated about pinning, structural changes, and sub-phases associated with the SDW ground state to describe the data. For systems with magnetic field induced spin density wave states (FISDW), two thermopower studies to 30 T have done on the quasi-one dimensional organic conductor series $(TMTSF)_2ClO_4$[26] and $(TMTSF)_2PF_6$ under pressure[27]. In these materials a FISDW transition occurs from a Q1D metallic state to a sequence of SDW states. Both the MTEP and Nernst signals, which bear some relation to the corresponding transport measurements (i.e. longitudinal resistivity ρ_{xx} and the Hall effect ρ_{xy} respectively), are sensitive to these transitions. As the final FISDW sub-phase is entered at constant field with lower temperatures, the thermopower first rises with an activated (gap-like) behavior, followed by a decrease at lower temperatures deeper in the SDW phase. The behavior is interpreted in terms of collective modes within the SDW phases. Notably, quantum oscillations (the so-called "rapid oscillations" which are periodic in inverse field) are observed in the thermopower for both materials. These experiments show the usefulness of thermopower measurements to probe ground states that are induced at high magnetic fields.

In this paper, we report thermopower measurement results carried out under high magnetic field and at low temperatures in α-(BEDT-TTF)$_2$KHg(SCN)$_4$. The heat current was applied along all three crystallographic axes, and the longitudinal (Seebeck coefficient) and the transverse (Nernst-Ettinghausen effect) thermopower was measured. The asymptotic behaviors of the Seebeck coefficient and the Nernst-Ettinghausen effect suggest that the magnetic breakdown of the closed orbit in the reconstructed Fermi surface are responsible for the observed behavior of magnetothermopower.

III. EXPERIMENT

α-(BEDT-TTF)$_2$KHg(SCN)$_4$ single crystal samples were obtained from the conventional electrochemical crystallization technique. The orientation of crystallographic axes were determined from polarized IR reflection measurements at room temperature. Three different samples from a single batch were used for each three different experimental conditions (heat current $\parallel$ a-axis, c-axis or b-axis). The magnetic field was always applied along the least conducting axis (b-axis). When the heat current was applied in the most conducting plane (ac-plane), off-diagonal term of thermopower tensor (S_{yx}) was also measured simultaneously. The polarity of magnetic field was switched for the measurement of S_{yx} to remove spurious components due to the misalignment of the voltage leads. (The alignment of voltage leads for S_{xx} measurements was also checked in this manner.) Thermopower measurements were carried out by applying sinusoidal heat currents along a crystallographic axis of the single crystal and measuring thermal emf along the same direction and along the direction rotated by 90 degrees. (see Fig. 1 (c)) The sample was mounted between two quartz blocks, which were heated by sinusoidal heating currents (with oscillation frequency f_0 = 66 mHz) with $\pi/2$ phase difference. The corresponding temperature gradient (∇T) and thermal emf with $2f_0$ oscillation frequency were measured. The magnetothermopower of Au lead wires was in situ calibrated by $YBa_2Cu_3O_{7+\delta}$ superconductor. To avoid an ambiguity in determination of ∇T under magnetic field, we exploit the reproducibility of ∇T, which only weakly depends on magnetic field. The procedures of the magnetothermopower measurement method used in this work are detailed elsewhere[28].

IV. RESULTS AND DISCUSSION

A. Zero field thermopower

The temperature dependence of zero field thermopower results For α-(BEDT-TTF)$_2$KHg(SCN)$_4$, along each of the principal axes is shown in Fig. 2, where the inset shows low temperature expansion near T_p = 8 K. The in-plane results are in general agreement with previous measurements by Mori et al.[16], as discussed in Sect. II. The negative (positive) sign of thermopower along the $a(c)$-axis indicates that the Fermi surface is electron (hole)-like along the $a(c)$-axis, which corresponds to the Fermi surface as shown in Fig. 1: here, for a thermal gradient along the c-axis direction, the hole pockets should contribute, whereas for the a-axis direction, the electron-like open orbits should contribute as well. We note however, that the temperature dependence of the TEP shown in Fig. 2 is non-monotonic. There is a minimum in S^c and S^a around T = 120 to 150 K .This behavior can be explained by applying the two-dimensional tight binding parameters for this material to the Boltzmann transport equation[16],[17].

The inter-plane TEP (S^b), perpendicular to the conducting planes, which has not been previously measured, shows a monotonic decrease until 35 K, where it changes sign. The positive sign of S^b above T = 35 K indicates that the hole-like carriers are dominant for the inter-layer transport above T = 35 K and the electron-like carriers dominate below that temperature. Clearly, the inter-plane transport shows a distinctly different behavior to that of the in-plane TEP.

From the linear dependence of S^c and S^b at higher temperature, the density of states per carriers are derived to be 5.3 states/eV for S^c and 7.6 states/eV for S^b. The deviation from the linear dependence in the intermediate temperature range has been treated[16,17] by Mori et al., as mentioned in Sect. II above, as has the peak in S^c near 25

K . The peak in S^c may arise from the energy-dependent scattering term of Eq. 1, or from the phonon drag effect. The TEP associated with phonon drag results from the electron-phonon coupling. The temperature dependence changes from a T^3 to a T^{-1} behavior[12] with increasing temperature. Especially, peak structures at low temperature (typically between $\theta_D/10$ and $\theta_D/5$, where θ_D is the Debye temperature) are usually attributed to the phonon drag effect, whose temperature dependence in noble metals is quite similar to that of S^c. Thermopower measurements on the other members of this compound (α-(BEDT-TTF)$_2$MHg(SCN)$_4$, where M=Tl, Rb, NH_4) also showed peak structures at lower temperatures (15 $\sim$ 20 K), which were attributed to the phonon drag effect[29]. Of note is the superconductivity of the NH_4 salt, where there is an enhancement of density of states and effective mass (m* $\approx 2.1m_0$ for κ-(BEDT-TTF)$_2$$NH_4$Hg(SCN)$_4$ over that of non-superconducting α-(BEDT-TTF)$_2$KHg(SCN)$_4$ (m* $\approx 1.5m_0$)), as pointed out by Mori et al.[16] However, the origin of enhancement of m*, which may be due to electron-electron interaction and/or electron-phonon interaction, is not yet clear.

When the heat current is applied perpendicular to the most conducting planes, the 2D band model will not be appropriate without considering the energy dispersion between conducting planes. Since simple mixing of two contributions of S^a and S^c cannot produce temperature dependence and magnitude of S^b, it is necessary to find a proper model for inter-plane transport. A straightforward application of the $S \approx T/W$ relationship produces unrealistic values of the b-axis bandwidth (of order 250 meV), which is known from Fermiology studies to be at least 100 times smaller. At present there is no satisfactory treatment of either the magnetoresistance or the thermopower for the b-axis transport behavior.

The behavior of the thermopower through the density wave transition (T_p= 8 K) has also not been previously reported. From the inset of Fig. 2, jumps of thermopower for S^a and S^c are observed near the metal-density wave transition temperature (T_p). In the resistance measurements, the change of slope near T_p may be attributed to the vanishing conductivity of the open orbit band (σ_{1D}) in parallel with the remaining finite conductivity of closed orbit band (σ_{2D})[30]. In addition, for thermopower measurements, metallic carriers give a linear T-dependence while activation over a band gap gives a $1/T$ dependence. Therefore for one type of carrier (either from open orbit or closed orbit) exclusively, S^a will diverge below T_p. Experimentally, there is always the possibility of random diffusion of heat along the sample due to misalignment between heat currents and crystal axes, and also, the total thermopower may involve a mixing of contributions from several bands (especially below T_p where the Fermi surface is reconstructed). Nevertheless, we believe that dominant behavior of thermopower in the present case reflects the influence of the heat currents with respect to the topology and orientation of the specific orbits.

When two types of carriers are involved, the total thermopower can be written as[11],

$$S_{tot} = \frac{\sigma_{1D}S_{1D} + \sigma_{2D}S_{2D}}{\sigma_{1D} + \sigma_{2D}} \quad (2)$$

Above T_p, both orbits have metallic conductivity and thermopower; hence the total thermopower shows a linear temperature dependence. But below T_p, a band gap opens for $1D$ band, therefore σ_{1D} goes to zero exponentially as the temperature decreases, and S_{1D} diverges as $1/T$. However, below this temperature, a modified closed orbit band remains, which still gives a metallic thermopower contribution. Consequently, just below the transition temperature, there will be a jump of thermopower, ΔS, from the divergence of S_{1D}, but this contribution quickly disappears as σ_{1D} goes to zero.

We may further compare the magnitude of jump of thermopower (ΔS) and that of electronic heat capacity (ΔC_{el}). Since thermopower measures heat carried by a carrier divided by the carrier charge and temperature, ΔS equals $\Delta C_{el}/e$. Adding both contributions from S^a and S^c, ΔS is about 1 μV/K, which corresponds to $\frac{1}{6.24}$ $\times 10^{-24}$ J/ K·carrier. The reported ΔC_{el} is about 0.1 J/mol·K[31] and 0.25 J/mol·K[32], which are in fair agreement with ΔS. A corresponding change in S^b at T_p is unclear, if it exists at all (in Fig. 2). This indicates that the phase transition around T_p = 8 K occurs predominantly within the in-plane electronic structure.

B. Magnetothermopower

In Fig. 3, we present the magnetic field dependence of the TEP (i.e. MTEP) for all three crystallographic directions at different, fixed temperatures. To show the field dependence more clearly, some traces are offset from zero as indicated by the dashed lines. The MTEP signal contains two components, the background MTEP which is sensitive to the Fermi surface topology, and the oscillatory MTEP which is a manifestation of the Landau quantization of the closed orbit Fermi surface. To separate the two signals, we show in Fig. 4 the background MTEP data where the oscillatory MTEP has been removed by filtering the total MTEP signal. Finally, the Nernst-Ettinghausen effect at different temperatures is shown in Fig. 5. In all cases the magnetic field is applied along the b-axis, perpendicular to the $a-c$ conducting plane.

A similarity between the magnetic field dependence of the thermopower and the resistance can be expected from the Boltzmann transport equations. Indeed we find that the general field-dependence of the MTEP is similar in some respects to that of the magnetoresistance[4]: (1) Below T_p, the in-plane MTEP shows a broad peak at $B(= B_A) \sim 10$ T. (2) Above the "kink field" B_k at 22.5 T, the field dependence is weak. (3) Quantum oscillations are observed in the MTEP signal associated with the de Haas-van Alphen (dHvA) and Shubnikov - de Haas (SdH)

effects (i.e., from Eqn. 1, both thermodynamic and transport properties are involved in the thermopower). The oscillation amplitudes are largest for S^c_{xx}, and the oscillations are also observed in S^b_{zz}. (4) The MTEP also shows hysteresis for up and down field sweeps.

Beyond the general comparison between resistivity and MTEP, unique field-dependent features are observed in the MTEP and Nernst signals: (1) For S^a_{xx} and S^c_{xx}, the MTEP exhibits a minimum at $B = B_{min}$ after which it rapidly increases up to maximum at $B = B_A$. B_{min} is also temperature dependent, and decreases with increasing temperature.

(2)For the a-axis behavior, the Nernst signal S^a_{yx} shows a similar field dependence to the MTEP signal S^a_{xx} in general, but S^a_{yx} is asymptotic to zero above B_k for all temperatures measured. In contrast, S^a_{xx} is asymptotic to non-zero, temperature dependent values above B_k.

(3) For the c-axis behavior, S^c_{yx} shows linear field dependence at higher field, which is distinct from the other thermopower coefficients.

(4) For the b-axis, S^b_{zz} exhibits some aspects of S^a_{xx} and S^c_{xx} mentioned above, which may involve some mixing of the in-plane components.

Fig. 6 shows the temperature dependence of magnetothermopower for fixed magnetic field. As the magnetic field is increased, the transition temperature T_p, represented as a jump or shoulder in the data, shifts to lower temperature. (For S^b_{zz} and S^c_{xx} at B=27 T however, T_p could not be resolved.) The temperature-field phase diagram, based exclusively on the field and temperature dependent thermopower data (B_{min}, B_A, B_K, and $T_p(B)$), is shown in Fig. 7. The phase diagram is very similar (with the exception of the new B_{min} line) to previous determinations by transport[33,39], NMR[34,35], magnetization[8,37], and specific heat[36].

1. *Theoretical aspects of high field thermopower measurements*

To interpret the origin of the field dependence of the MTEP, it is useful to examine the magnetic field dependence of the thermopower for an anisotropic system. When thermopower is measured under magnetic field, tensor elements of thermopower should be considered since both the temperature gradient and the magnetic field are vectorial. For our experimental conditions (zero electric current and zero transverse heat current), the kinetic equations for thermopower and heat currents can be written as,

$$E_i = \alpha_{ij}\nabla T_j, \qquad (J_q)_i = -K_{ij}\nabla T_j \tag{3}$$

where E is the electric field produced by the thermal emf, α is the thermopower tensor under magnetic field, J_q is the heat current, and K is the thermal conductivity tensor. We have two different experimental situations.

(a) $H \parallel z-$ axis $\parallel J_q \parallel \nabla T_z$ (S^b_{zz} in this paper) : In this case, no Lorentz force is applied so that $\nabla T_x = \nabla T_y = 0$, and above equations have simple scalar form,

$$E_z = \alpha_{zz}\nabla T_z, \qquad (J_q)_z = -K_{zz}\nabla T_z \tag{4}$$

The measured value S^b_{zz} is obtained from $E_z/\nabla T_z$.

(b) $H \parallel z-$ axis $\perp J_q$ (S^a_{xx}, S^a_{yx}, S^c_{xx} and S^c_{yx} in this paper) : In this case, ∇T is not parallel with J_q, and has a non-zero y component given by -$\nabla T_x K_{yx}/K_{yy}$. If we rewrite Eq. 3 for this case,

$$\begin{pmatrix} E_x \\ E_y \end{pmatrix} = \begin{pmatrix} \alpha_{xx} & \alpha_{xy} \\ \alpha_{yx} & \alpha_{yy} \end{pmatrix} \begin{pmatrix} \nabla T_x \\ -\nabla T_x K_{yx}/K_{yy} \end{pmatrix} \tag{5}$$

In terms of measured values, Eq. 5 can be expressed as,

$$S_{xx} = \frac{E_x}{\nabla T_x} = \alpha_{xx} - \alpha_{xy}\frac{K_{yx}}{K_{yy}}$$

$$S_{yx} = \frac{E_y}{\nabla T_x} = \alpha_{yx} - \alpha_{yy}\frac{K_{yx}}{K_{yy}} \tag{6}$$

The asymptotic behavior of thermoelectric tensor α_{ij}[15] and thermal conductivity tensor K_{ij}[14] were calculated at low temperature and high magnetic field. They show different behavior for the three different cases, i.e., (a) closed and compensated orbits (b) closed and uncompensated orbits and, (c) open orbits along the $x-$direction. For each case, the asymptotic behaviors of S_{ij} can be calculated and the results are summarized in Table I.

The saturation values are temperature dependent for each case, and they should be determined by considering the scattering and the dispersion relations.

2. *Comparison of theoretical and experimental MTEP results*

We now compare the thermopower data with the theoretical field dependence described above. We focus our attention on the behavior of the S^c signal shown in Fig. 3 and 4, since it is significantly larger than the other signals, and it is predominantly hole-like (i.e. positive, and closed orbit-sensitive). We may use as a guide the detailed work by Uji et al. on the Fermiology study of the quantum oscillations[45], due to closed orbits in the magnetic breakdown network, which have been proposed to describe the Fermi surface topology below T_p. In this model it is assumed that only small closed orbit pockets exist in the reconstructed Fermi surface below T_p near zero magnetic field. As the magnetic field is increased, larger and larger Fermi surface sections become involved in the SdH oscillations as magnetic breakdown becomes more probable. These effects appear experimentally in the SdH measurements: in Figs. 8 and 9 of Ref. [45], the onset of the SdH oscillations associated with the various

magnetic breakdown orbits (α, ϕ, etc.) occurs above 3.5 T. At higher fields, above 7 T, the β orbit associated with the Brillouin zone appears, i.e. magnetic breakdown occurs over most of the Fermi surface. Finally, above the kink field, the original Fermi surface topology (as in Fig. 1) re-emerges.

In light of the above, our first point of comparison is the behavior of B_{min}. For S^c, and indeed in all MTEP directions, there is a distinct change in the signal above B_{min} from a relatively flat response to a pronounced increase in slope (approximately linear) with field. This behavior is entirely consistent with the theoretical model above for a set of closed, compensated orbits.

At higher fields, above B_A, the compensated closed orbit behavior of S^c changes dramatically, and this indicates that the magnetic breakdown network of closed orbits is undergoing modification with increasing field. By comparison with the theory above, we may speculate that this is the onset of uncompensated closed orbit behavior, which exhibits less (eventually no) field dependence.

Finally, above the kink field, the original, uncompensated closed orbit FS is realized, and the field dependence disappears, as is evident from the S^c data. Above B_K, we may compare the temperature dependence of S^c with those at zero field above T_p (See Fig. 6). Except for field dependent offsets, the thermopower above $T_p(B)$ for the three directions is similar, save for the case of S^b which is anomalous, even in the absence of field.

Beyond this simple comparison of the most dominant MTEP signal with previous SdH studies and theoretical expectations, the assignment the mechanisms responsible for the magnetic field dependence of S^a and S^b are more speculative. This is due to the apparent mixing of terms in the experimental data, and to sort them out is beyond the scope of the present work. However, the Nernst data shows significant difference for the a and c axes (S^a_{yx} and S^c_{yx}). This is most apparent above B_k, where the original FS is expected to be recovered. Here S^a_{yx} is seen to be asymptotic to zero (i.e. H^{-1} dependence), whilst S^c_{yx} clearly assumes a linear (i.e. H^1) dependence. This behavior is consistent with expectations based on the theory represented in Table 1.

3. MTEP and Landau quantization

From Eq. 1, it is clear that for a quasi-two dimensional Fermi surface, the magnetic field dependence of the Landau level spectrum[41] will produce quantum oscillations in the thermopower, which will originate from both thermodynamic and electron transport factors. The latter has been treated by Zil'berman[42] and Long et al.[43] where scattering between states of the Landau level closest to the Fermi surface and states of other occupied are considered. We find in our results a clear indication of the Landau level spectrum in the MTEP and Nernst data, the periodicity of which is in good agreement with previous SdH and dHvA measurements[44]. In particular, the oscillation frequency obtained from the fast Fourier transform (FFT) analysis of S^c_{xx} and S^c_{yx} at 0.7 K (see Fig. 8) is about 667 T, which agrees with results obtained from other measurements[45]. This comparison also includes the observation of higher harmonics of the fundamental α orbit, and even the ϕ orbit (180 T) which is expected to be a manifestation of the magnetic breakdown topology below B_k. (See for instance Uji et al.[45]).

An important feature of our results, most evident above B_k, is a phase difference between the METP and Nernst quantum oscillations. This is shown in Fig. 9 for two different cases, the a-, and c-axes. Indeed, Zil'berman's model[42,43] predicts a phase difference of π between the MTEP and Nernst oscillations. We show this more explicitly for S^c_{xx} andS^c_{yx} at T=0.7 K in Fig. 10 , with the angle (θ) defined as the ratio of the electric fields due to transverse and longitudinal thermopower (θ=arctan (S_{yx}/S_{xx})= arctan(E_y/E_x). The phase difference is π, which supports Zil'berman's model[42].

Zil'berman's model also predicts similar field and temperature dependence of oscillation amplitude with that of the Lifschitz-Kosevich formula for de Haas-van Alphen oscillations. The amplitude of thermopower oscillation increases when $B_A < B < B_k$, but it is almost field independent above B_k. We note that in this range of temperature, the quantum oscillation amplitude is complicated due to the anomalous high field state, where the dHvA and SdH behave in a significantly different manner, and a comparison based on standard LK theory is not applicable. A more systematic study of the MTEP and Nernst effects above B_k vs temperature, and also vs. field orientation, will be necessary to provide a complete picture.

V. CONCLUSION

We have applied the method of magnetothermopower to investigate the low temperature, magnetic field dependent phase of the anisotropic organic conductor α-(BEDT-TTF)$_2$KHg(SCN)$_4$. Our results show that the sensitivity of thermopower to anisotropic Fermi surface topologies may be extended to the study of systems where temperature and magnetic field alter these topologies. The most significant results of the present investigation include the determination of the low temperature phase diagram of α-(BEDT-TTF)$_2$KHg(SCN)$_4$, based purely on thermopower measurements, the study of the onset of magnetic breakdown effects via the magnetothermopower, and the measurement of quantum oscillations in the magnetothermopower and Nernst effect, which are in accord with theoretical expectations.

Acknowledgments

This work was carried out at the National High Magnetic Field Laboratory, which is funded by a cooperative agreement between the National Science Foundation and the State of Florida through NSF-DMR 00-84173. JSB acknowledges support from NSF-DMR-99-71474 for this work, and ESC acknowledges post-doctoral support from KOSEF.

---

* Present address: Physics Dept., Wake Forest University, Winston-Salem, NC 27109
999]

[1] H. Mori. S. Tanaka, M. Oshima, G. Saito, T. Mori, Y. Maruyama, and H. Inokuchi, Bull. Chem. Soc. Jpn., **63**, 2183 (1990).

[2] M.V. Kartsovnik, A.E. Kovalev and N.D. Kushsch, J. Phys. I France **3**, 1187 (1993).

[3] M.V. Kartsovnik and V.N. Laukin, J. Phys. I France **6**, 1753 (1996).

[4] T. Sasaki, A.G. Lebed, T. Fukase, and N. Toyota, Phys. Rev. B **54**, 12969 (1996).

[5] J. S. Qualls, L. Balicas, J. S. Brooks, N. Harrison, L. K. Montgomery and M. Tokumoto, Phys. Rev. B **62**, 10008 (2000).

[6] C. Proust, A. Audouard, A. Kovalev , D. Vignolles, M. Kartsovnik, L. Brossard, and N. Kushch, Phys. Rev. B **62**, 2388 (2000).

[7] T. Osada, R. Yagi, A. Kawasumi, N. Miura, M. Oshima and G. Saito, Phys. Rev. B **41**, 5428 (1990).

[8] N. Harrison, L. Balicas, J.S. Brooks, M. Tokumoto, Phys. Rev. B **62**, 14212 (2000).

[9] N. Harrison, C. H. Mielke, A.D. Christianson, J. S. Brooks, M. Tokumoto, Phys. Rev. Lett., **86**, 1586 (2001).

[10] N. A. Fortune, M.A. Elben, S. Uji, H. Aoki, J. Yamada, S. Tanaka, S. Make, S. Nakatsuji, H. Anzai, Synth. Met. **103**, 2078-2079 (1999).

[11] D. K. C. Mcdonald, *Thermoelectricity*, John Wiley & Sons, New York, 1962.

[12] P.M. Chaikin, in *Organic Superconductivity*, V.Z. Kresin and W.A. Little, Eds., Plenum Press, New York, pp101-115, 1990.

[13] I. M. Lifshitz, M. Ya. Azbel and M. I. Kaganov, Soviet Physics JETP **4**, 41 (1957).

[14] M. Ya. Azbel, M. I. Kaganov and I. M. Lifshitz, Soviet Physics JETP **5**, 967 (1957).

[15] Yu. A. Bychkov, L. É. Gurevich and G. M. Nedlin, Soviet Physics JETP **37**, 377 (1960).

[16] T. Mori, H. Inokuchi, H. Mori, S. Tanaka, M. Oshima and G. Saito, J. Phys. Soc. Jpn. **59**, 2624-2626 (1990).

[17] T. Mori and H. Inokuchi, J. phys. Soc. Jpn. **57** 3674 (1988).

[18] R. C. Yu, J. M. Williams, H. H. Wang, J. E. Thompson, A. M. Kini, K. D. Carlson, J. Ren, M.-H. Whangbo, and P. M. Chaikin, Phys. Rev. B **44**, 6932-6936 (1991).

[19] S. Gartner, E. Gogu, L. Heinen, H.J. Keller, T. Klutz, and D. Schweitzer, Solid State. Commun., **65**, 1531 (1988).

[20] Buravov, L.I.; Kushch, N.D.; Merzhanov, V.A.; Osherov, M.V.; Khomenko, A.G.; Yagubskii, E.B. Journal de Physique I **2** 1257 (1992).

[21] P. M. Chaikin, R. L. Greene, S. Etemad and E. Engler, Phys. Rev. B **13**, 1627 (1976),

[22] P. M. Chaikin, J. F. Kwak and A. J. Epstein, Phys. Rev. Lett., **42**, 1178 (1979).

[23] K. Bender, D. Schweitzer, and H.J. Keller, Journal de Physique Colloque C3, **44** 1433-1436 (1983).

[24] G. Yu. Logvenov, M.V. Karsovnik, H. Ito, and T. Ishiguro, Synt. Met. **86**, 2023-2024 (1997).

[25] V.A. Bondarenko, S. Kagoshima, M. Maesato, T. Hasegawa, N. Miura, and T. Yamaguchi, Solid State Commun. **107** 477 (1998).

[26] R.C. Yu, L. Y. Chiang, R. Upasani and P. M. Chaikin, Phys. Rev. Lett. **65**, 2458 (1992).

[27] W. Kang, S. T. Hannahs, L. Y. Chiang, R. Upasani and P. M. Chaikin, Phys. Rev. B **45**, 13566 (1992).

[28] E. S. Choi, J. S. Brooks, J. S. Qualls and Y. S. Song, Rev. Sci. Inst. June (2001); Los Alamos Preprint Library: physics/0009054.

[29] S. V. Demishev, M.V. Kondrin, V.V. Glushkov, N.E. Sluchanko, and N.A. Samarin, JETP **86**, 182 (1998)[Zh.Eksp.Teor. Fiz. **113**, 323 (1998)].

[30] J.S. Brooks, G. J. Athas, S. J. Klepper, X. Chen, C. E. Campos, S. Valfells, Y. Tanaka, T. Kinoshita, N. Kinoshita, M. Tokumoto and H. Anzai, Physica B **201**, 449 (1994).

[31] A. Kovalev, H. Mueller and M. V. Kartsovnik, JETP **86**, 578 (1998).

[32] P. F. Henning, J. S. Brooks, J. E. Crow, Y. Tanaka, T. Kinoshita, N. Kinoshita M. Tokumoto and H. Anzai, Sol. Stat. Comm. **95**, 691 (1995).

[33] N. Biskup, J. A. A. J. Perenboom, J. S. Brooks and J. S. Qualls, Solid State Commun. **107**, 503 (1998).

[34] K. Miyagawa, A. Kawamoto and K. Kanoda, Phys. Rev. B 56, R8487(1997)

[35] P. Kuhns, J. S. Brooks, T. Caldwell, W. G. Moulton, A. P. Reyes, N. Biskup, A. M. Kini, J. A. Schlueter, H. H. Wang, U. Geiser and J. M. Williams, Solid State Commun. 109, 637 (1999).

[36] A. Kovalev, H. Mueller,M.V. Kartsovnik, JETP 113, 1058(1998).

[37] M.V. Kartsovnik, W. Biberacher, E. Steep, P. Christ, K. Andres, A.G.M Jansen, and H. Mueller, Synthetic Metals, 86 1933 (1997).

[38] R. Mckenzie, G. J. Athas, J. S. Brooks, R. G. Clark, A. S. Dzurak, R. Newbury, R. P. Starrett, A. Skougarevsky, M. Tokumoto, N. Kinoshita, T. Kinoshita and Y. Tanaka, Phys. Rev. B **54**, R8289 (1996).

[39] T. Sasaki, S. Endo and N. Toyota, Phys. Rev. B **48**, 1928 (1993).

[40] V. N. Topnikov, S. I. Pesotskii and V. N. Laukhin, JETP Lett. **59**, 374 (1994).

[41] I. M. Lifshitz and A. M. Kosevich, Soviet Physics JETP **2**, 636 (1957).

[42] G. E. Zil'berman, Soviet Physics, JETP **2**, 650 (1956).

[43] J. R. Long, C. G. Grenier and J. M. Reynolds, Phys. Rev. **140**, A187 (1965).

[44] J. Wosnitza, *Fermi Surfaces of Low-Dimensional Organic Metals and Superconductors*, Springer Verlag, Berlin-

Heidelberg 1996.
[45] S. Uji, T. Terashima, H. Aoki, J. S. Brooks, M. Tokumoto, N. Kinoshita, T. Kinoshita, Y. Tanaka and H. Anzai, Phys. Rev. B **54**, 9332 (1996).

TABLE I: High field power law behavior (H^γ where γ = 1,0, -1) of the magnetothermopower for different types of orbits

	closed compensated	closed uncompensated	open along the $x-$direction
K_{yx}/K_{yy}	H^0	H^1	H^{-1}
α_{xx}, α_{yy}	H^1	H^0	H^0
α_{xy}	H^1	H^{-1}	H^1
α_{yx}	H^1	H^{-1}	H^{-1}
α_{zz}	H^0	H^0	H^{-1}
S_{xx}	H^1	H^0	H^0
S_{yx}	H^1	H^1	H^{-1}
S_{zz}	H^0	H^0	H^0

FIG. 1: Fermi surface of α-(BEDT-TTF)$_2$KHg(SCN)$_4$ (a) prior to and (b) after reconstruction. **q** denotes nesting vector. (c) Lead wire configuration for magnetothermopower and Nernst effect measurements.

FIG. 2: Temperature dependence of zero field thermopower of α-(BEDT-TTF)$_2$KHg(SCN)$_4$ when the temperature gradient is applied along the a-axis ($S^a, *$), c-axis ($S^c, \circ$) and b-axis ($S^b, \triangle$). The inset shows the low temperature behavior near the transition temperature T_p.

FIG. 3: Magnetothermopower of (a) S^a, (b) S^c and (c) S^b for field down sweeps. Field sweep up data are also shown for T $\sim$ 1.5 K. The arrows indicate characteristic fields as defined in the text. Shifted zeros for some data sets are indicated by dashed lines. For unshifted data, see Fig. 4

FIG. 4: Background magnetothermopower of S^a and S^b obtained from Fig. 3 by filtering out the quantum oscillation component.

FIG. 5: Nernst effect of α-(BEDT-TTF)$_2$KHg(SCN)$_4$when the heat current is applied along a-axis (S^a_{yx}) and c-axis (S^c_{yx}).

FIG. 6: Temperature dependence of magnetothermopower of α-(BEDT-TTF)$_2$KHg(SCN)$_4$ measured under fixed magnetic field. Arrows indicate the transition temperature T_p.

FIG. 7: T-B Phase diagrams of α-(BEDT-TTF)$_2$KHg(SCN)$_4$ drawn from S^a_{xx} and S^c_{xx}. T_p is obtained from the temperature sweep and B_{min}, B_A and B_K are obtained from the field sweep. Empty symbols are from S^a_{xx} and filled symbols from S^c_{xx}.

FIG. 8: FFT spectrum for S^c_{xx} and S^c_{yx} at T=0.7 K and 1.5 K for 8.6 T $\leq B \leq$ 12 T and 8.6 T $\leq B \leq$ 27 T. The fundamental frequency of the closed hole orbit (α orbit) and its higher harmonics are clearly shown. The peak at 180 T is the ϕ orbit, as in Ref.[45]

FIG. 9: Transverse and longitudinal magnetothermopower oscillation as a function of inverse magnetic field in the high field region for (a) S^a and (b) S^c. The background magnetothermopower was subtracted and the amplitude of S^c_{xx} was divided by 5.

FIG. 10: Comparison of the phases of oscillations between S^c_{xx} and S^c_{yx} at T= 0.7 K and plot of arctan(S^c_{xx}/S^c_{yx}) as a function of magnetic field.

(a)

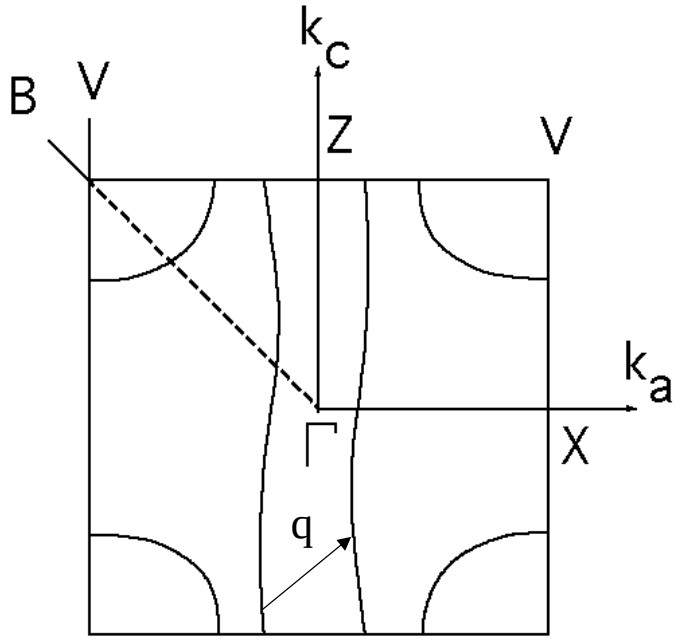

(b)

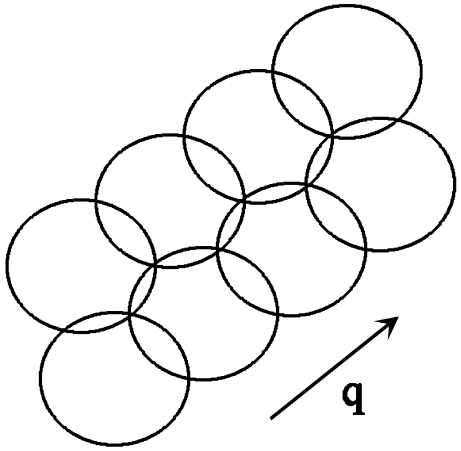

(c)

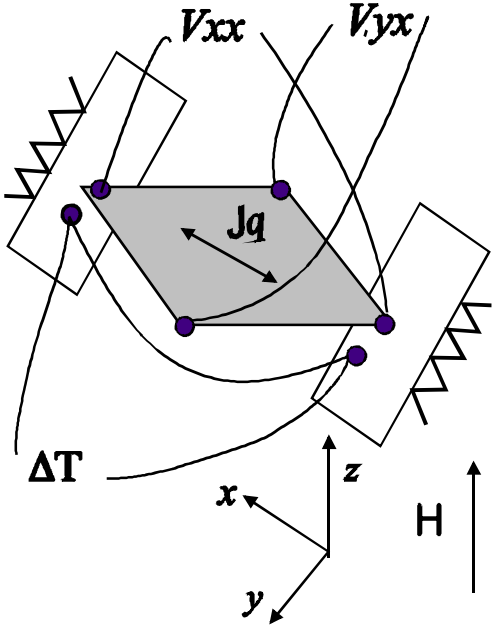

$Sxx = Vxx/\Delta T$

$Syx = Vyx/\Delta T$

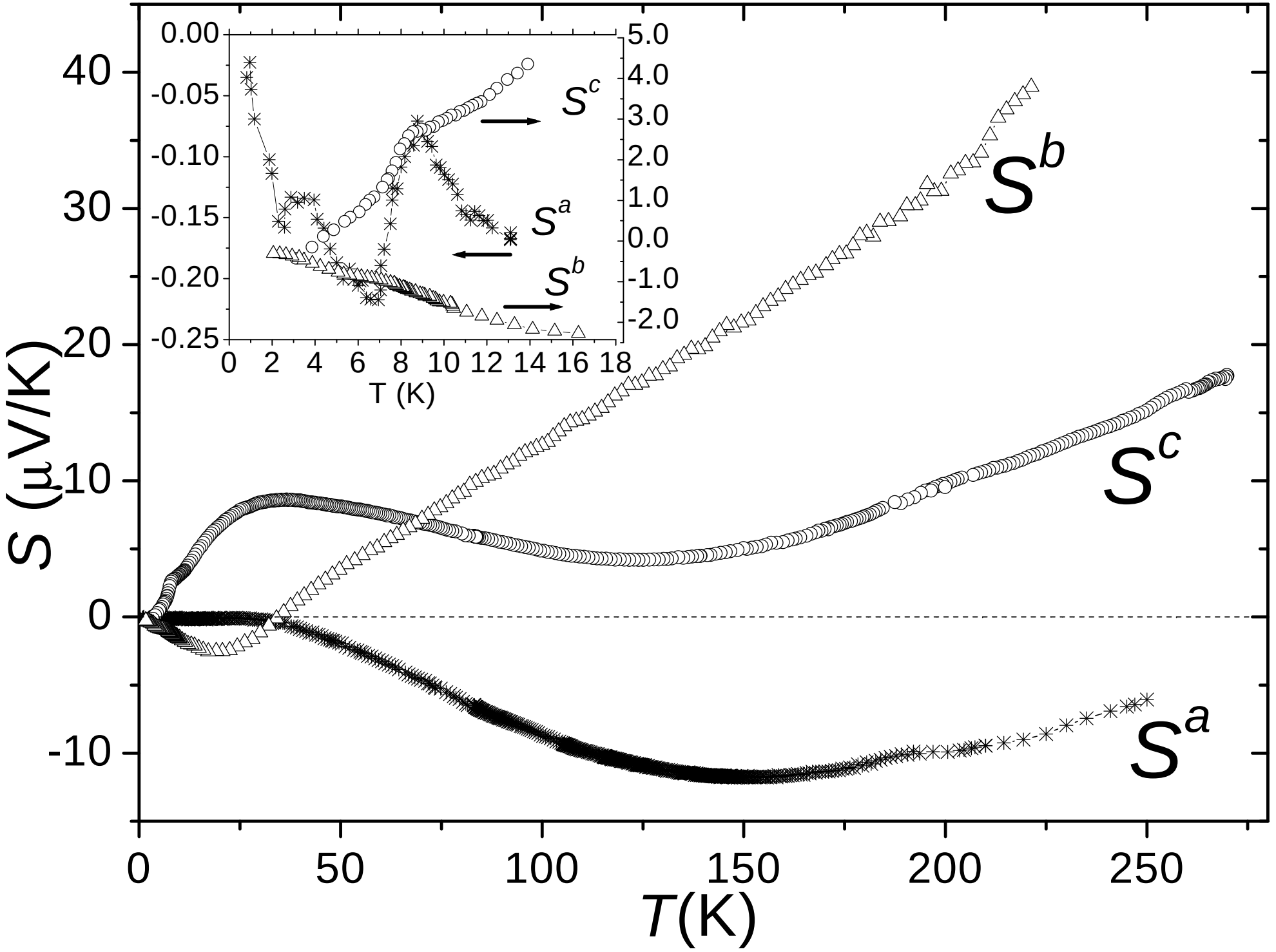
S (μV/K)
T (K)
S^b
S^c
S^a
0.00
-0.05
-0.10
-0.15
-0.20
-0.25
5.0
4.0
3.0
2.0
1.0
0.0
-1.0
-2.0
0 2 4 6 8 10 12 14 16 18
T (K)
S^c
S^a
S^b
40
30
20
10
0
-10
0 50 100 150 200 250
T(K)

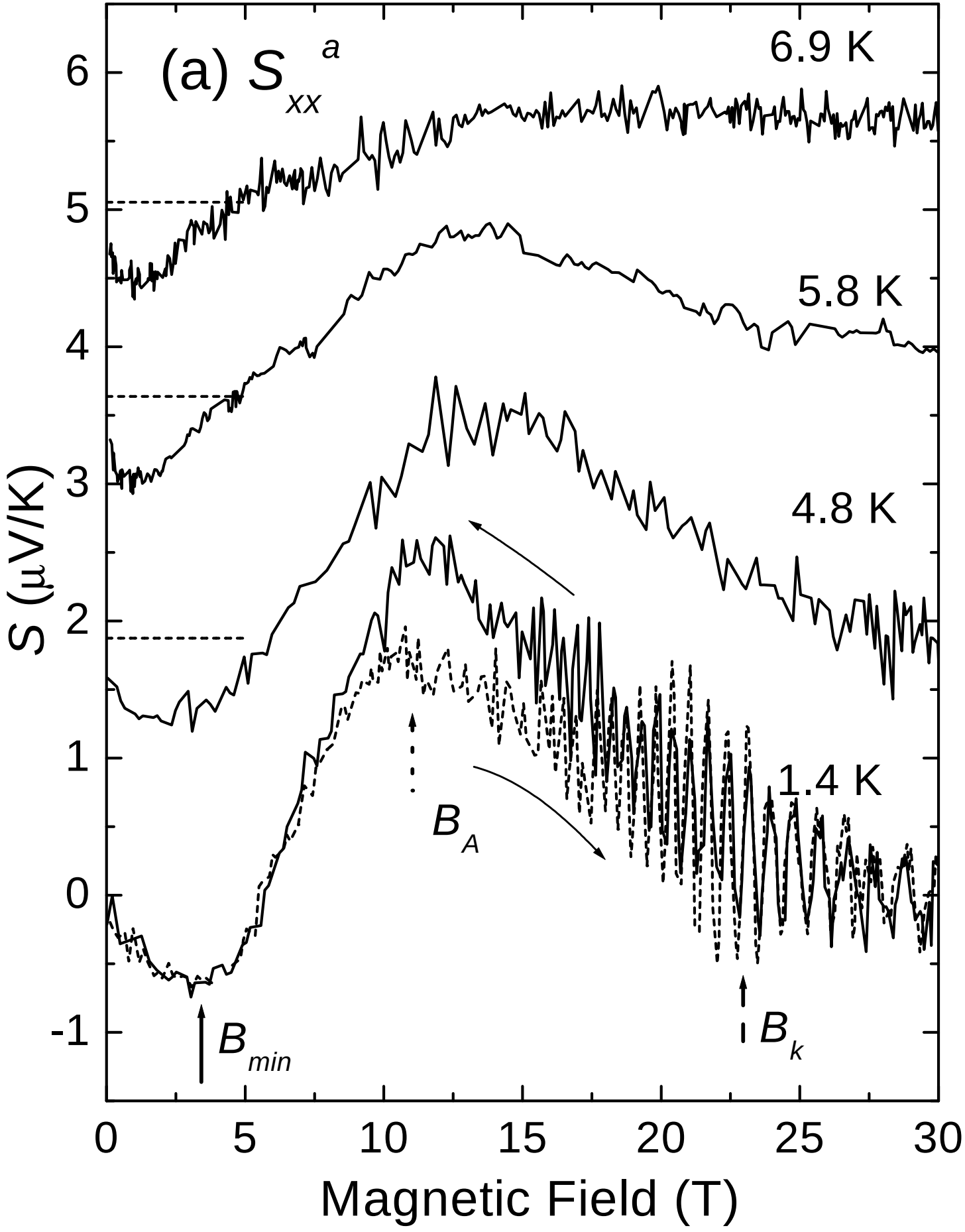
(a) S_{xx}^{a}
6.9 K
5.8 K
4.8 K
1.4 K
B_{min}
B_A
B_k
S (μV/K)
Magnetic Field (T)
6
5
4
3
2
1
0
-1
0
5
10
15
20
25
30

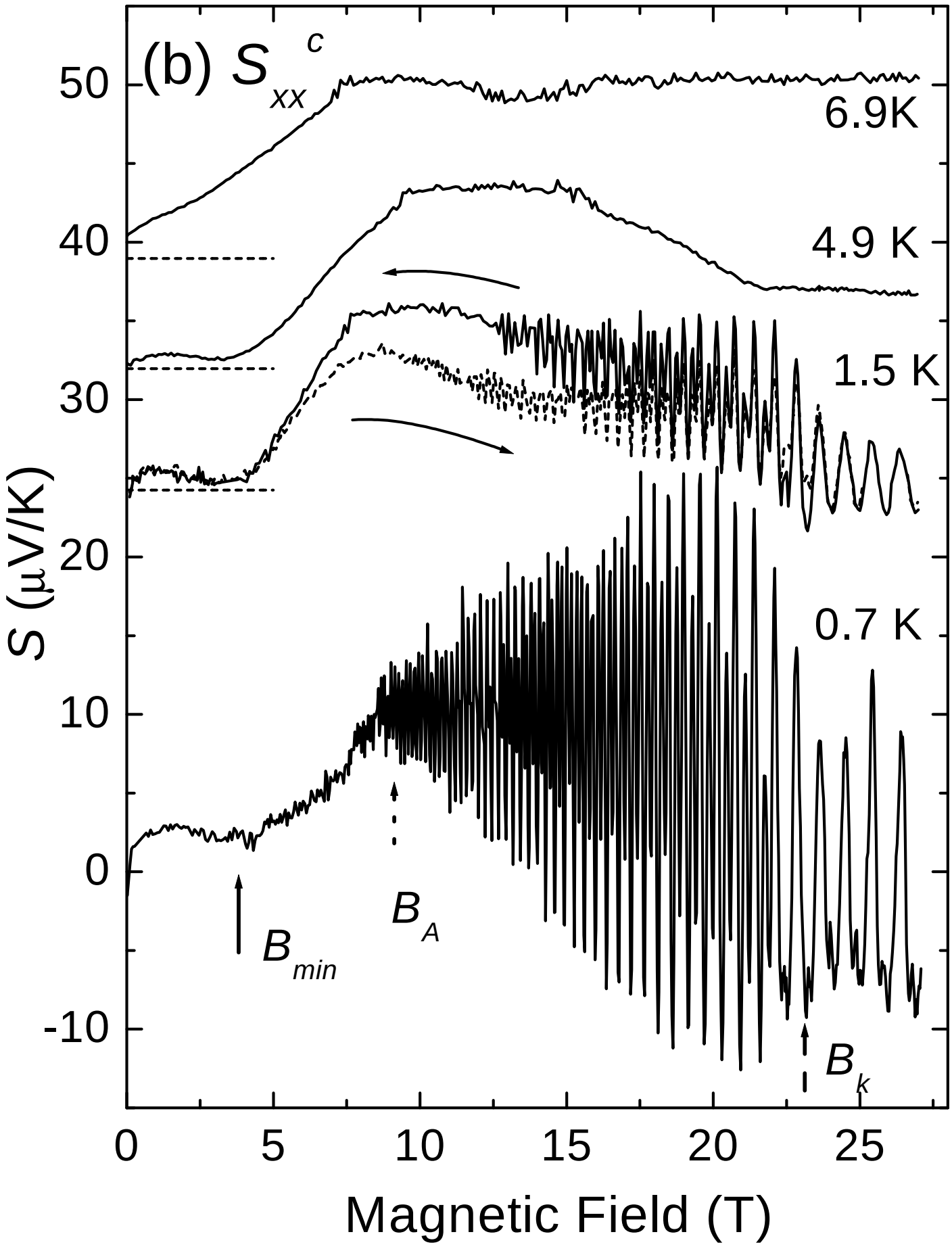
(b) S_{xx}^{c}
6.9K
4.9 K
1.5 K
0.7 K
B_{min}
B_A
B_k
S (μV/K)
Magnetic Field (T)
50
40
30
20
10
0
-10
0
5
10
15
20
25

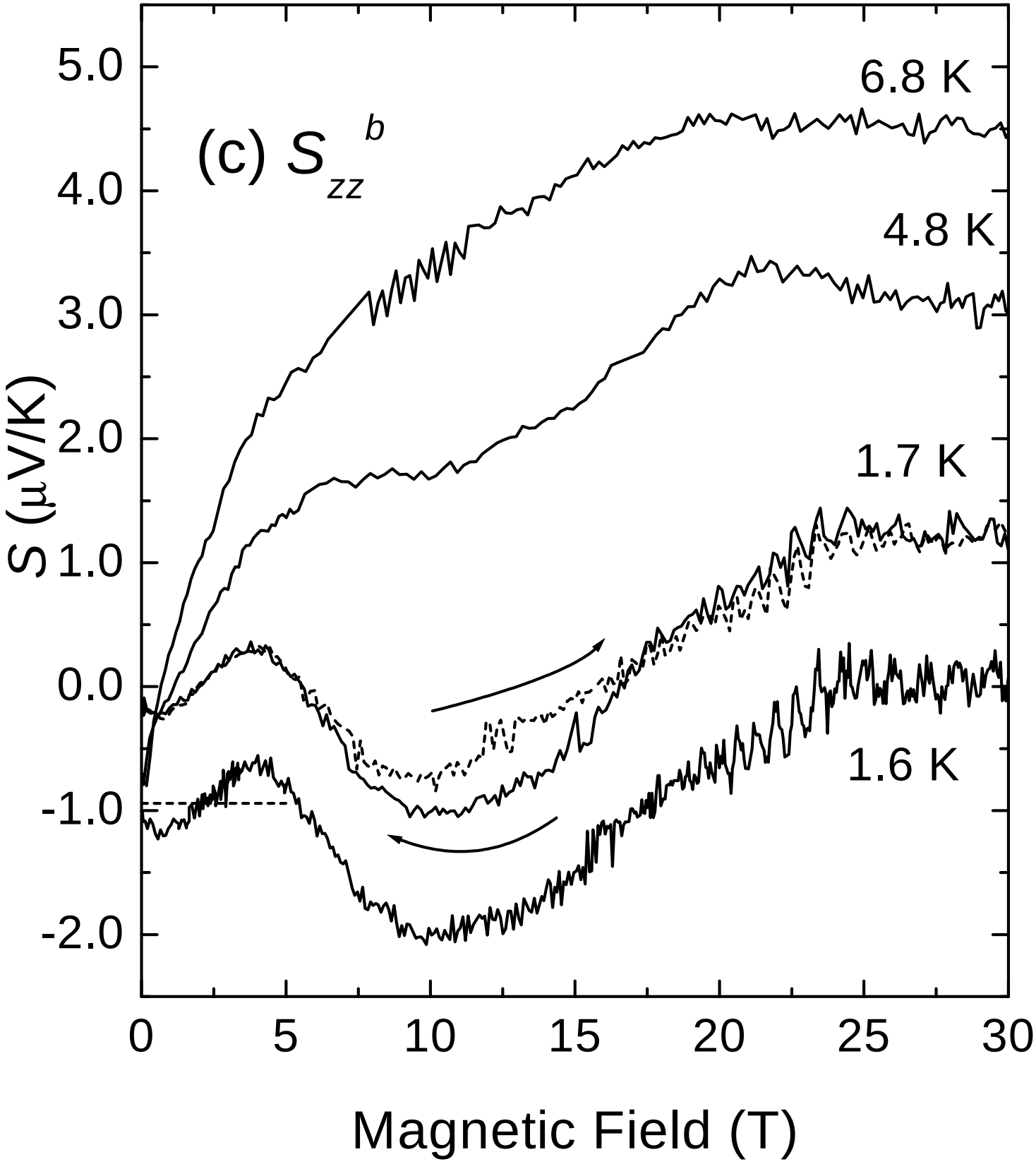
(c) S_{zz}^{b}
6.8 K
4.8 K
1.7 K
1.6 K
S (μV/K)
5.0
4.0
3.0
2.0
1.0
0.0
-1.0
-2.0
0
5
10
15
20
25
30
Magnetic Field (T)

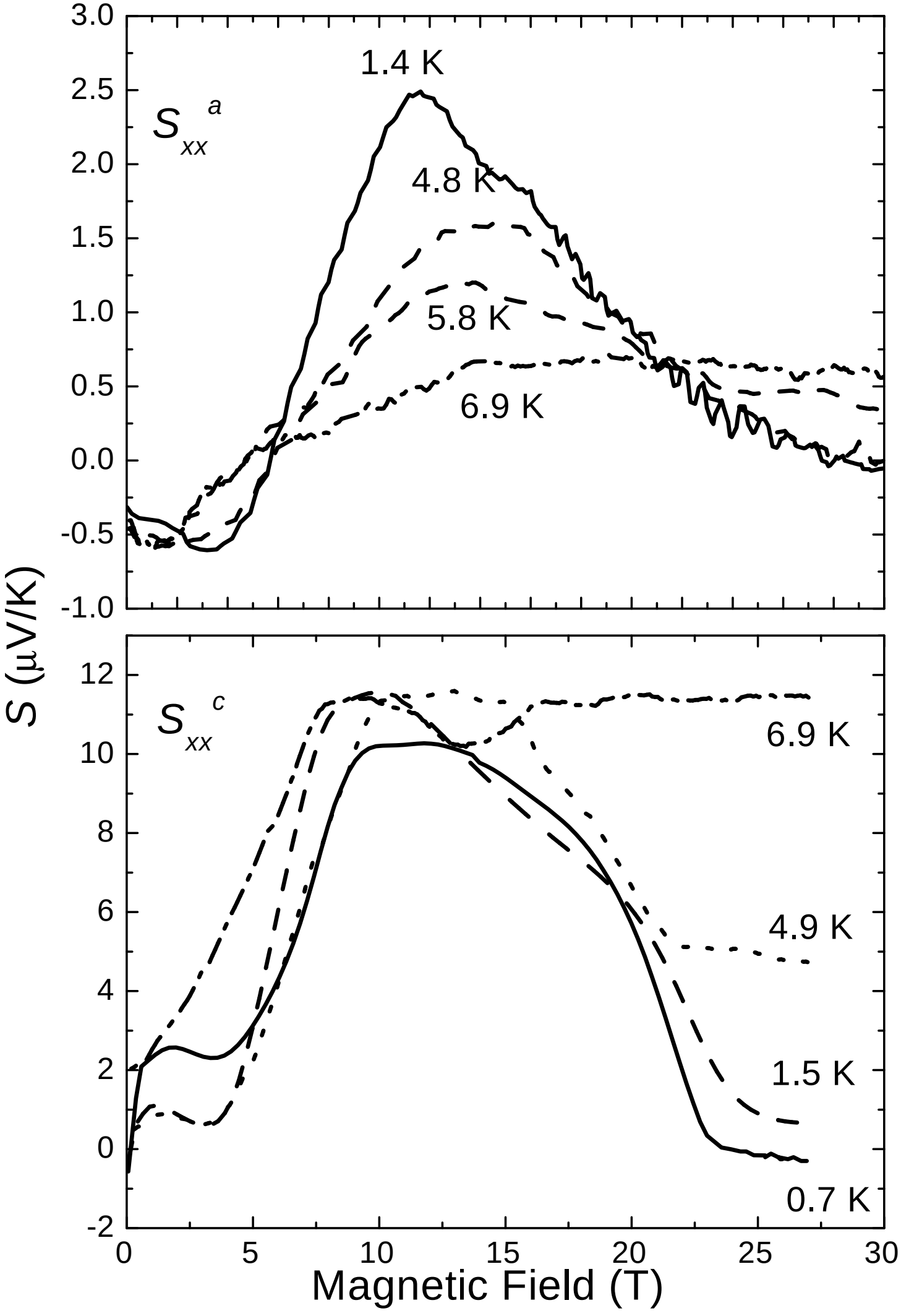
3.0
2.5
2.0
1.5
1.0
0.5
0.0
-0.5
-1.0
1.4 K
S_{xx}^{a}
4.8 K
5.8 K
6.9 K
12
10
8
6
4
2
0
-2
S_{xx}^{c}
6.9 K
4.9 K
1.5 K
0.7 K
S (μV/K)
0
5
10
15
20
25
30
Magnetic Field (T)

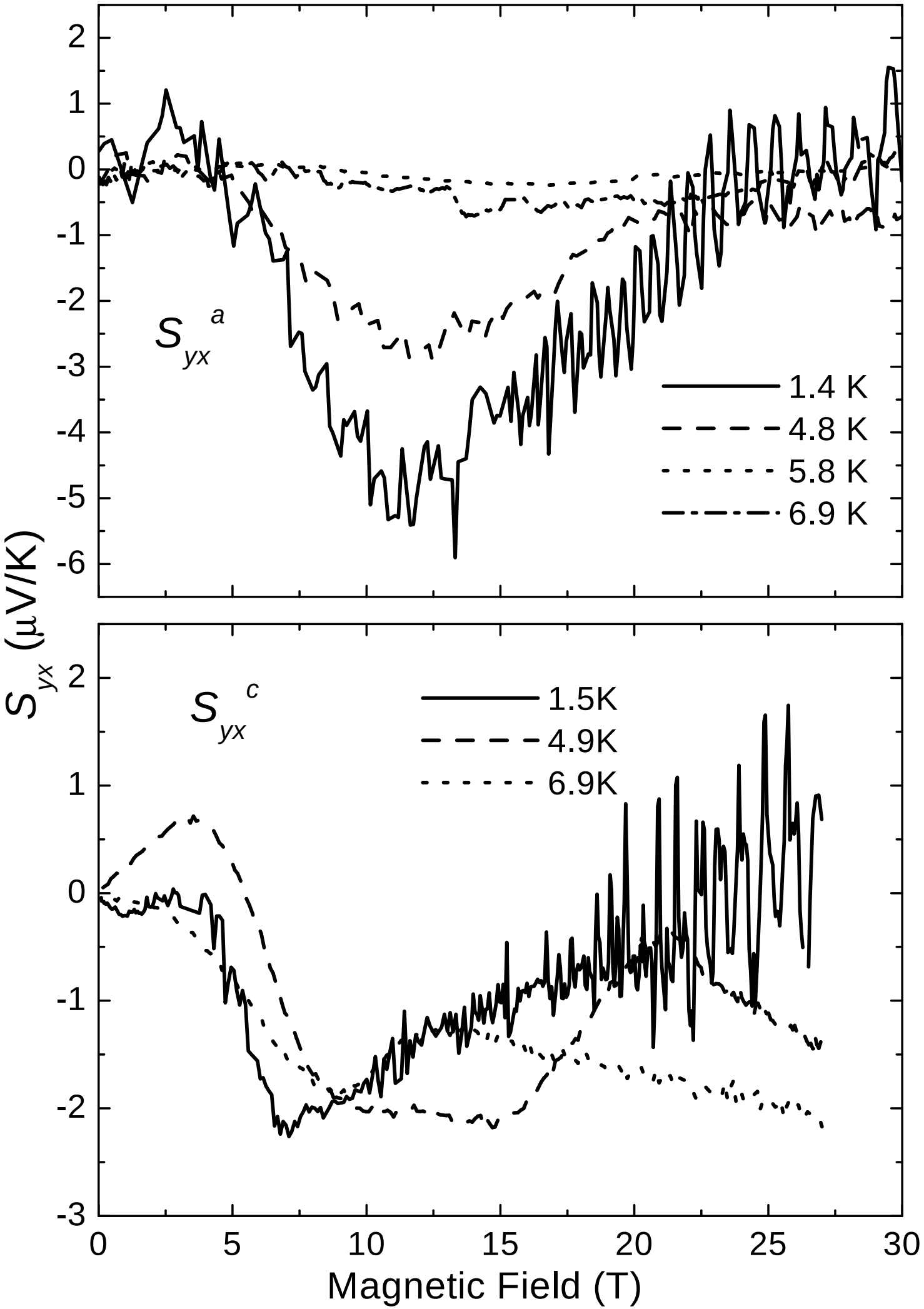
S_{yx}^{a}
1.4 K
4.8 K
5.8 K
6.9 K
S_{yx}^{c}
1.5K
4.9K
6.9K
S_{yx} (μV/K)
Magnetic Field (T)
2
1
0
-1
-2
-3
-4
-5
-6
0
5
10
15
20
25
30

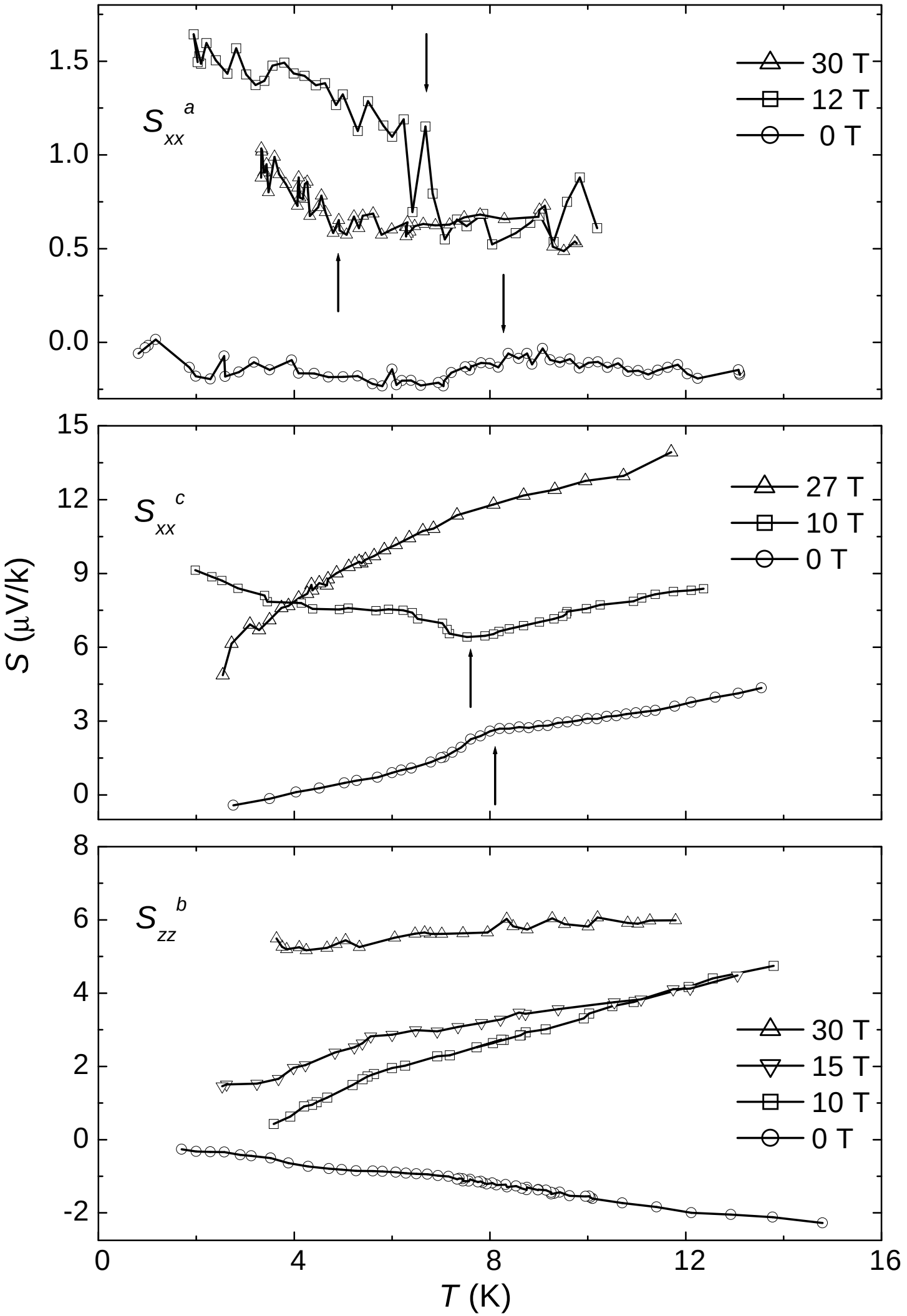
S_{xx}^{a}
30 T
12 T
0 T
S_{xx}^{c}
27 T
10 T
0 T
S_{zz}^{b}
30 T
15 T
10 T
0 T
S (μV/k)
T (K)
1.5
1.0
0.5
0.0
15
12
9
6
3
0
8
6
4
2
0
-2
0
4
8
12
16

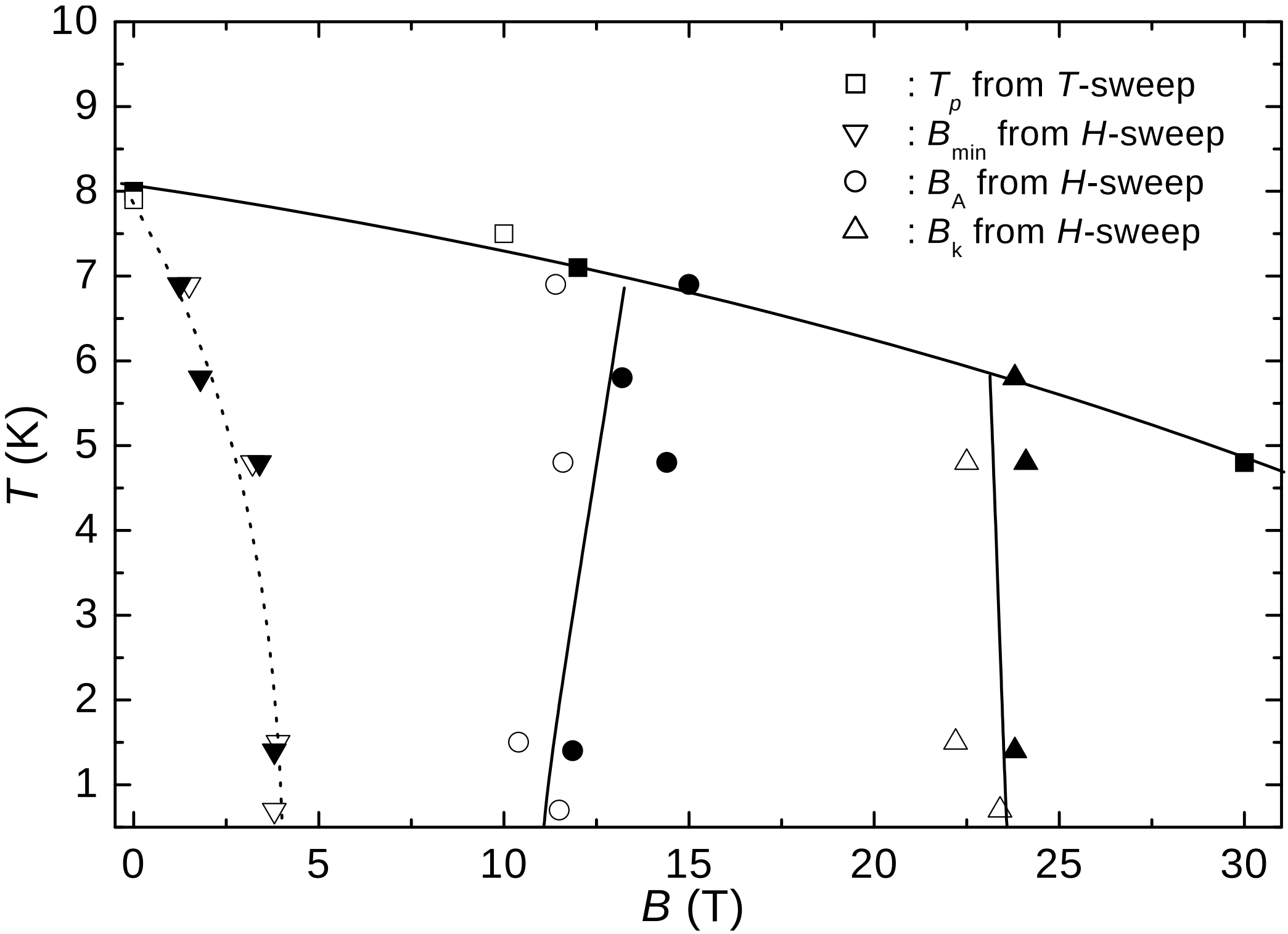
□ : T_p from T-sweep
▽ : B_{min} from H-sweep
○ : B_A from H-sweep
△ : B_k from H-sweep
T (K)
B (T)
0
5
10
15
20
25
30
1
2
3
4
5
6
7
8
9
10

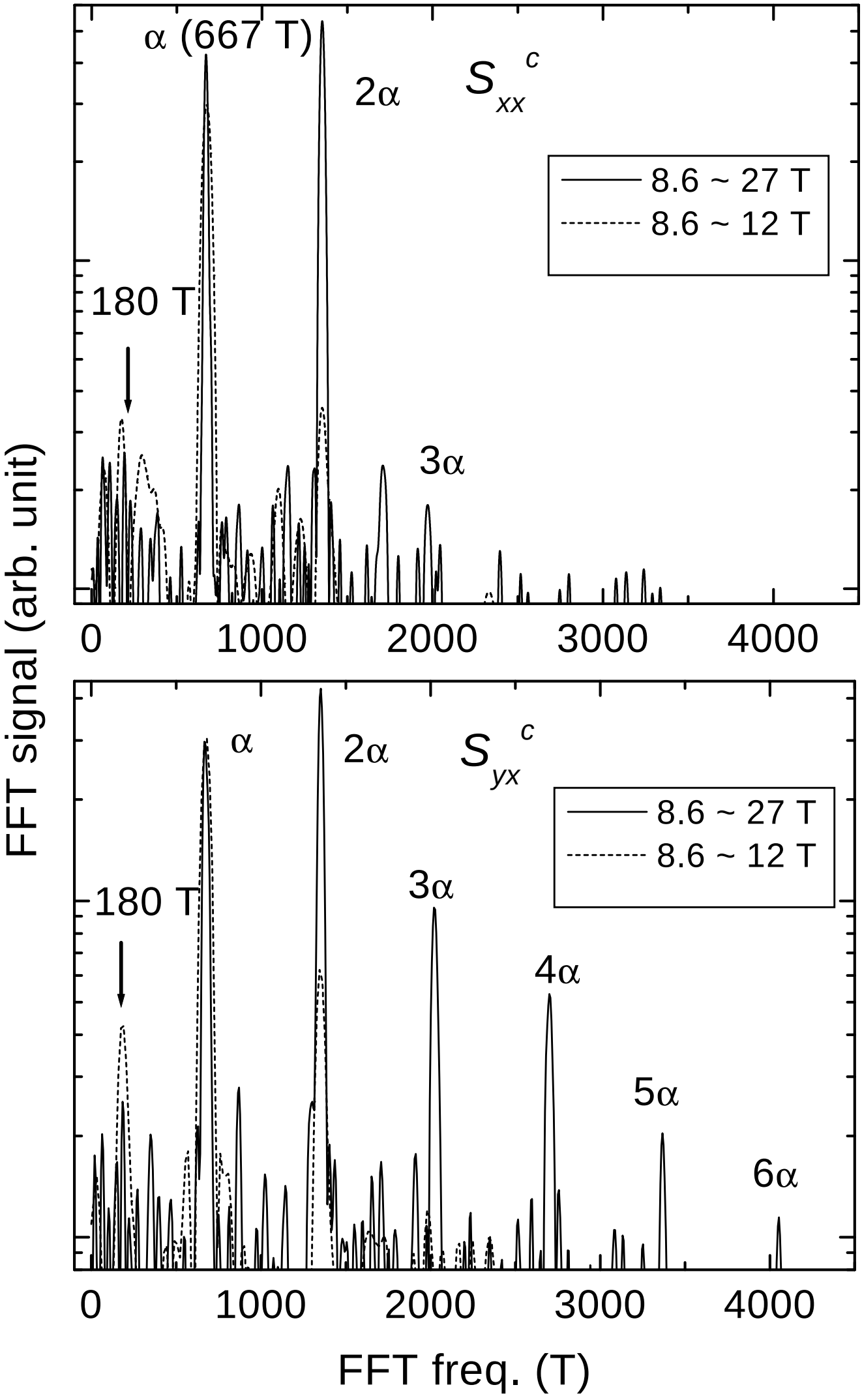
α (667 T)
2α
S_{xx}^{c}
8.6 ~ 27 T
8.6 ~ 12 T
180 T
3α
0
1000
2000
3000
4000
α
2α
S_{yx}^{c}
8.6 ~ 27 T
8.6 ~ 12 T
180 T
3α
4α
5α
6α
0
1000
2000
3000
4000
FFT signal (arb. unit)
FFT freq. (T)

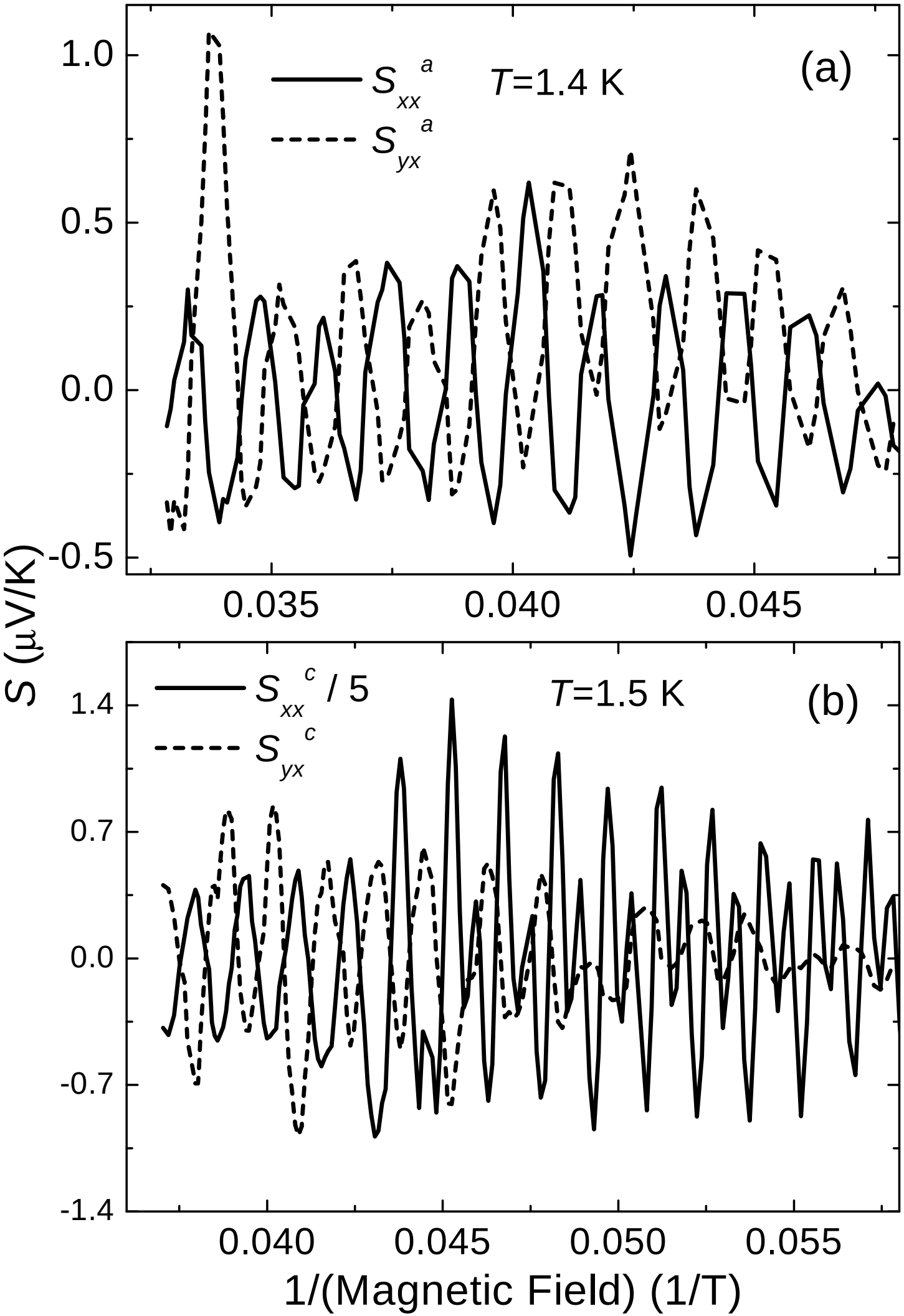
(a)
S_{xx}^{a}
S_{yx}^{a}
T=1.4 K
1.0
0.5
0.0
-0.5
0.035
0.040
0.045
(b)
S_{xx}^{c} / 5
S_{yx}^{c}
T=1.5 K
1.4
0.7
0.0
-0.7
-1.4
0.040
0.045
0.050
0.055
S (μV/K)
1/(Magnetic Field) (1/T)

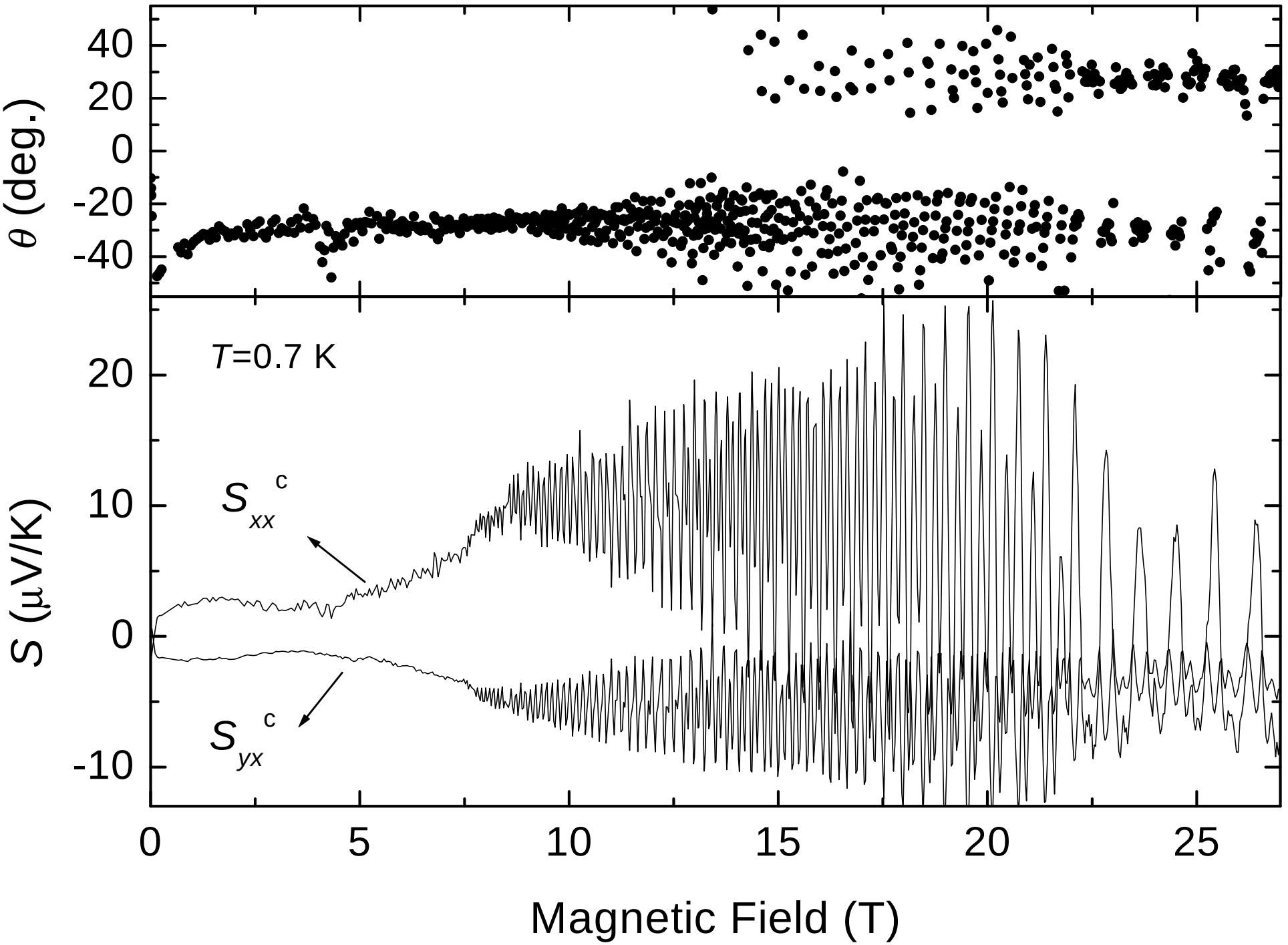
θ (deg.)
40
20
0
-20
-40
T=0.7 K
S (μV/K)
20
10
0
-10
S_xx^c
S_yx^c
0
5
10
15
20
25
Magnetic Field (T)